The Astrophysical Journal Letters, 975:L4 (8pp), 2024 November 1 https://doi.org/10.3847/2041-8213/ad7ba7

Dust in Little Red Dots

Caitlin M. Casey[1,2], Hollis B. Akins[1,4], Vasily Kokorev[1], Jed McKinney[1,5], Olivia R. Cooper[1,4], Arianna S. Long[1,5], Maximilien Franco[1], and Sinclaire M. Manning[3,5]
[1] The University of Texas at Austin, 2515 Speedway Blvd Stop C1400, Austin, TX 78712, USA; cmcasey.astro@gmail.com
[2] Cosmic Dawn Center (DAWN), Denmark
[3] Department of Astronomy, University of Massachusetts Amherst, 710 N Pleasant Street, Amherst, MA 01003, USA
Received 2024 July 6; revised 2024 September 2; accepted 2024 September 14; published 2024 October 22

Abstract

JWST has revealed a ubiquitous population of "little red dots" (LRDs) at $z \gtrsim 4$, selected via their red rest-frame optical emission and compact morphologies. They are thought to be reddened by dust, whether in tori of active galactic nuclei (AGNs) or the interstellar medium, though none have direct dust detections to date. Informed by the average characteristics of 675 LRDs drawn from the literature, we provide ballpark constraints on the dust characteristics of the LRD population and estimate they have average dust masses of $\langle M_{\rm dust}\rangle = (1.6^{+4.8}_{-0.9}) \times 10^4\ M_\odot$, luminosities of $\langle L_{\rm IR}\rangle = (8^{+3}_{-5}) \times 10^{10}\ L_\odot$, and temperatures of $\langle T_{\rm dust}\rangle = 110^{+21}_{-36}$ K. Notably, the spectral energy distributions are thought to peak at ∼100 K (rest-frame 20–30 μm) regardless of heating mechanism, whether AGN or star formation. LRDs' compact sizes $R_{\rm eff} \sim 100$ pc are the dominant factor contributing to their low estimated dust masses. Our predictions likely mean LRDs have, on average, a submillimeter emission factor of ∼100× fainter than current Atacama Large Millimeter/submillimeter Array limits provide. The star-to-dust ratio is a factor ∼100× larger than expected from dust formation models if one assumes the rest-optical light is dominated by stars; this suggests stars do not dominate. Despite their high apparent volume density, LRDs contribute negligibly (0.1%) to the cosmic dust budget at $z \gtrsim 4$ due to their low dust masses.

Unified Astronomy Thesaurus concepts: AGN host galaxies (2017); Dust continuum emission (412); James Webb Space Telescope (2291)

1. Introduction

A key discovery of JWST's first few years has been the remarkable ubiquity of a population of $z \gtrsim 4$ compact "little red dots" (LRDs; I. Labbe et al. 2023; J. Matthee et al. 2024). The population is characterized by compact (spatially unresolved) morphologies and red rest-frame optical colors. Many also have a faint, blue component in the rest-frame ultraviolet (UV), resulting in a characteristic "V-shaped" spectral energy distribution (SED).[6] The population of LRDs at $z \gtrsim 4$ is surprisingly common, with volume densities $\gtrsim 10^{-5}$ Mpc^{-3}, making up a few percent of the galaxy population at these epochs. Yet a similar population at low z—both compact and red—seems not to exist or is orders of magnitude more rare (D. D. Kocevski et al. 2023).

The first spectra of the population (J. E. Greene et al. 2024; D. D. Kocevski et al. 2023; J. Matthee et al. 2024) revealed that nearly all LRDs (∼80%) have broad Balmer lines (Hα and Hβ with FWHM $\gtrsim 2000$ km s^{-1}) consistent with a direct view of the broad-line region of a luminous active galactic nuclei (AGN). Such broad-line systems are typically seen alongside blue rest-frame UV continuum emission from the accretion disk (R. Antonucci 1993; B. M. Peterson 2006; R. C. Hickox & D. M. Alexander 2018) as both are spatially coincident (the broad-line region is on the order of light days and immediately adjacent to the accretion disk on astronomical unit scales); where one is seen, so is the other. The juxtaposition of the red rest-frame optical colors of LRDs combined with broad lines marks a fundamental puzzle for our understanding of the physics of LRDs; one implies significant dust attenuation ($A_V \approx 2$–4), while the other seems inconsistent with such attenuation.

The presence of significant dust attenuation has a few important ramifications. First, the intrinsic luminosities of LRDs may be larger than observed; high intrinsic luminosities at high redshifts then increase potential tension with fundamental models of the formation of the first massive black holes and/or the galaxies around them. It then becomes important to understand the dominant source of the continuum emission in LRDs: is it from a reddened accretion disk or reddened starlight from the host galaxy? Where is the relevant dust—in a hot torus on ∼pc scales or in the ISM extended on ∼100 pc scales?

Answering these questions about LRDs is core to understanding why their volume densities are so high. If LRDs are dominated by AGN emission—both across all wavelengths and the full population—then they imply a tremendous overabundance of supermassive black holes, about 2 orders of magnitude (D. D. Kocevski et al. 2024; V. Kokorev et al. 2024) larger than was expected from pre-JWST observations of the bolometric quasar luminosity function (X. Shen et al. 2020). Alternatively, if starlight is contributing significantly to the continuum (B. Wang et al. 2024b), then several LRDs may push the limits of stellar mass assembly in ΛCDM (fundamentally limited by the cosmic baryon fraction times and the halo mass, $M_\star \leqslant f_{\rm b} M_{\rm halo}$, with very high stellar baryon fractions $\epsilon_\star \sim 0.3$–0.5).

[4] NSF Graduate Research Fellow.
[5] NASA Hubble Fellow.
[6] Some works explicitly select for the V-shaped SED as photometric redshifts are much better constrained with a detected rest-frame UV component (I. Labbe et al. 2023, 2023; D. D. Kocevski et al. 2024; V. Kokorev et al. 2024).

While the broad lines point to ubiquitous AGN,[7] there is evidence the continuum may not be from AGN. For example, a majority (>95%) of LRDs lack dominant hot dust emission (∼500–2000 K) from a torus, which may be expected at luminosities similar to the bolometric luminosity of the accretion disk itself (R. C. Hickox & D. M. Alexander 2018). It is suggested that such hot torus dust should be directly visible using JWST's MIRI instrument if the reddening in LRDs is due to torus dust. Current JWST/MIRI constraints of LRDs at >10 μm imaging largely show that LRDs have flat spectra in F_ν through the mid-IR, consistent with no torus emission (C. C. Williams et al. 2024; B. Wang et al. 2024a).

If the dust responsible for reddening the rest-optical spectra of LRDs is not in the form of >1000 K torus dust, then it must be present on scales of the interstellar medium (ISM) instead at significantly colder temperatures, perhaps as low as 30 K . Here we use the measured characteristics of LRDs to place boundary conditions on dust in LRDs. Section 2 presents the LRD samples we use, and Section 3 uses their characteristics to infer dust masses, luminosities, and temperatures. Section 4 presents predictions for the rest-UV through radio broadband SED of LRDs, Section 5 measures their dust mass density contribution, and Section 6 concludes.

2. Reference Samples of LRDs

We use two literature samples of LRDs in this work. The first is the LRD sample described in V. Kokorev et al. (2024; hereafter K24), selected across ∼640 arcmin^2 of JWST key extragalactic surveys including CEERS (# 1345; M. B. Bagley et al. 2023), PRIMER in COSMOS and UDS (# 1837), JADES (#1180, 1210, 1286, 1287; D. J. Eisenstein et al. 2023a, 2023b), and FRESCO (# 1895; P. A. Oesch et al. 2023) in GOODS-S and JEMS (# 1963; C. C. Williams et al. 2023). K24 describe the sample selection in detail in their Section 3.1; to summarize, it consists of a red color cut at $\lambda > 2$ μm (with either F200W − F356W > 1.0 or F277W − F444W > 0.7, depending on targeted redshift) and a moderately blue color cut between 1 μm < λ <2 μm (with either F115W − F150W < 0.8 or F150W − F200W < 0.8). Sources are also selected to be spatially unresolved in F444W. This results in a selection of 260 LRDs brighter than 27.7 AB in F444W.

The second LRD sample we use is from H. B. Akins et al. (2024; hereafter A24) selected over 0.50 deg^2 of the COSMOS-Web Survey (#1727; C. M. Casey et al. 2023). They present 434 LRDs brighter than 27.5 AB in F444W. The A24 selection is more extreme (requiring F277W − F444W > 1.5), and there is no explicit selection for a blue rest-frame UV slope (at 1 μm $\lesssim \lambda \lesssim$ 2 μm).

These two works are chosen here because of their large sample size, together consisting of 675 independently identified LRDs. Key differences between the samples are their redshift and color distributions; the K24 sample has a broader redshift distribution spanning $3 < z < 9$, while the A24 sample is restricted to $5 < z < 9$. This difference is largely due to the different color cuts (the red threshold is more extreme and filters more restrictive for the A24 sample). Figure 1 shows redshift versus A_V derived in both works, highlighting that the LRDs in A24 tend to be a bit redder, more highly attenuated, and higher redshift.

Another key difference is the approach to SED fitting in either work. K24 presumes all light (both continuum and emission lines) is dominated by an AGN, and therefore SED fitting is done using quasar templates. A24 uses both a set of galaxy templates and quasar templates to decompose the SEDs. We find that the magnitudes of extinction in the visual band, A_V, is consistent whether derived through galaxy or quasar templates. In other words, our results are agnostic to the SED methodology used to measure $z_{\rm phot}$, A_V, or the rest-frame absolute UV magnitude $M_{\rm UV}$ (calculated using A_V, $z_{\rm phot}$, and the photometry).

Despite their unresolved morphologies, the sizes of LRDs can be measured when detected at high signal to noise. Both K24 and A24 present size measurements in the F444W filter by assuming Sérsic (extended) light profiles. The inferred sizes are largely consistent, with mean sizes $\langle R_{\rm eff}\rangle = 91^{+22}_{-32}$ pc and $\langle R_{\rm eff}\rangle = 94^{+33}_{-72}$ pc, respectively (both smaller than the point-spread function, PSF). These measured sizes should be taken with a grain of salt; though they could be thought of as direct evidence of ISM-scale emission, Sérsic model fits to a control sample of stars results in statistically similar sizes. Additional uncertainty on the sizes may come from uncertainty in the PSF as well as the applicability of a Sérsic model. Nevertheless, we adopt the measured sizes at face value and will discuss how smaller (or larger) sizes may impact results.

The derived properties we use to constrain the dust characteristics of LRDs are:

1. A_V, which maps directly to a dust mass surface density, $\Sigma_{\rm dust}$, in the optically thin regime;
2. $R_{\rm eff}$, the half-light radius at F444W, used to map from dust mass surface density to total dust mass and also from dust mass and luminosity to dust temperature;
3. $M_{\rm UV}$, the rest-frame UV absolute magnitude, which can be used in conjunction with A_V to infer the reradiated dust luminosity;
4. Star formation rate (SFR) and $M_\star$ (measured only for the the A24 sample), which are used as a semi-independent check on the derived dust luminosity.

Section 3 presents the relevant scalings used to derive ballpark dust properties. Despite the differences in selection between the two LRD samples, the dust properties we estimate for either sample are similar.

3. Derivation of Dust Properties

Our goal is to place broad constraints on the dust properties of LRDs as a population. No LRDs have yet been detected via their dust emission in the millimeter, so here we derive their dust properties from observed JWST photometry in a back-of-the-envelope sense. Note that our derivation of dust mass, luminosity, and temperature is agnostic to AGN or stellar explanations for the LRD population. An exception to this is if the intrinsic sizes of LRDs are significantly smaller than the measured $R_{\rm eff} \sim 100$ pc, which would only *decrease* the dust mass and *increase* the dust temperature. The other exception is in the translation of dust luminosity and temperature into SEDs, the details of which differ based on the assumed energy source and are presented in Section 4.

[7] See J. F. W. Baggen et al. (2024), who argue that stellar kinematics could lead to broadened Balmer lines given the high stellar densities (P. F. Hopkins et al. 2010; I. Misgeld & M. Hilker 2011).

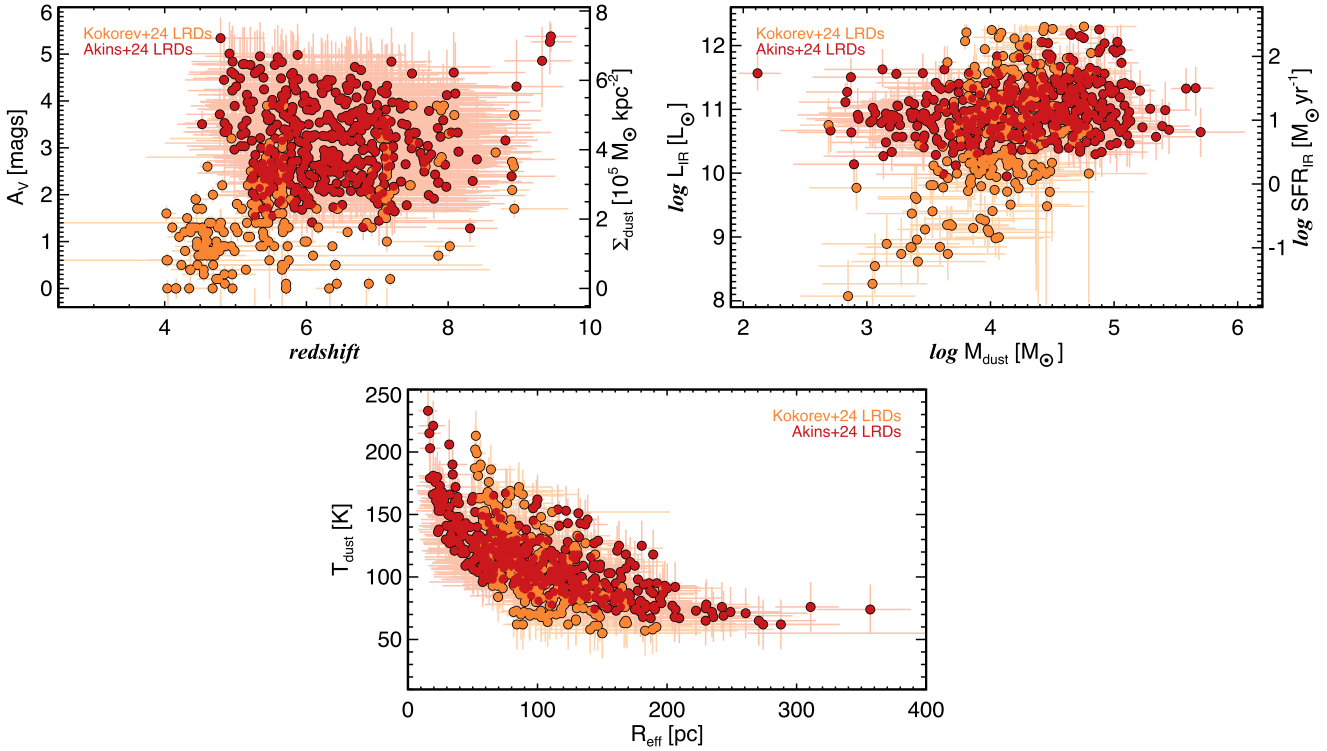

Figure 1. Top left: photometric redshift vs. visual magnitudes of extinction (A_V) inferred through SED fitting presented in K24 and A24. On the right y-axis we show the mapping from A_V to dust mass surface density using Equation (1). Top right: the estimated dust masses ($M_{\rm dust}$) and dust luminosities ($L_{\rm IR}$) for the sample. $L_{\rm IR}$ is agnostic to the source of emission (whether AGN or star formation), while $M_{\rm dust}$ depends on size and thus may be regarded as an upper limit. Bottom: reported size measurements for LRDs against the interpolated peak SED dust temperature, which is derived from the combination of $M_{\rm dust}$ and $L_{\rm IR}$.

3.1. Dust Masses

Absolute magnitudes of attenuation maps directly to dust (and gas) column density. We use the observed ratio of magnitudes of visual extinction to hydrogen column density, $A_V/N_{\rm H} = 5.34\times10^{-22}\,{\rm mag\,cm^2/H}$, consistent with measurements of X-ray observations of H column density and empirical optical extinction in the Milky Way (R. Bohlin et al. 1978; A. Diplas & B. D. Savage 1994; T. Güver & F. Özel 2009). B. Draine et al. (2007) present a range of dust-to-hydrogen mass ratios (in their Table 3); we adopt the canonical $M_{\rm dust}/M_{\rm H} = 0.01$ (where $M_{\rm H} = M({\rm H\,I} + {\rm H_2})$ and the dust-to-gas ratio, DGR, is equal to ${\rm DGR} = M_{\rm dust}/M_{\rm H}\times 1/1.36$ to account for the mass of helium). This should hold for an ISM enriched to $Z_\odot > 0.2$ (A. Rémy-Ruyer et al. 2014). This gives

$$A_V = 0.74\left(\frac{\Sigma_{\rm dust}}{10^5\,M_\odot\,{\rm kpc^{-2}}}\right){\rm mag}, \quad (1)$$

as given in B. T. Draine et al. (2014; see also G. Aniano et al. 2012). This corresponds to a uniform, foreground dust screen. We proceed with the scaling in Equation (1) but note that work on nearby galaxies (K. Kreckel et al. 2013) and distant obscured galaxies (J. A. Hodge et al. 2024) advocate for higher dust mass surface densities, which they fit empirically on physical scales >300 pc, finding $A_V = 0.18\Sigma_{\rm dust}/10^5\,M_\odot\,{\rm kpc^{-2}}$; this would result in $\Sigma_{\rm dust}$ a factor of $\sim4\times$ higher than we quote herein.

To derive a total dust mass, we multiply by an effective surface area $2\pi R_{\rm eff}^2$, found by integrating the $n=1$ Sérsic function in polar coordinates from $r = 0 - \infty$:

$$M_{\rm dust} = 2\pi R_{\rm eff}^2\,\Sigma_{\rm dust}. \quad (2)$$

The factor of 2 partially makes up for the simplicity of the foreground dust screen model by assuming double the dust mass (i.e., a screen in front and behind the illuminating source); the screen's density is assumed to fall off exponentially in the radial direction. These dust masses may be a factor of $\sim$2 lower than what is presumed using the K. Kreckel et al. (2013) A_V–$\Sigma_{\rm dust}$ scaling but within the same order of magnitude.

Ideally, one would have direct measurements of the effective surface area of dust emission, which may be different than the size of the system as inferred at 4.4 μm. Thus an implicit assumption is that the dust is absorbing light on the same physical scales of the ISM as measured via starlight in F444W.

We wish to emphasize that dust mass is most sensitive to the size measurement, $R_{\rm eff}$, and not the A_V–$\Sigma_{\rm dust}$ scaling. Because LRDs are inferred to be so compact (<300 pc), the dust masses do not exceed $10^5\,M_\odot$. There could, in principle, be a significant offset between measured near-IR size and the dust continuum size, as one might expect for highly obscured star-forming galaxies like dusty star-forming galaxies (DSFGs) where optically thick dust permeates the ISM, leaving only small channels of rest-frame UV/optical light to leak out where modest attenuation may be inferred (J. Howell et al. 2010; C. Casey et al. 2014b). However, we note that recent JWST imaging results of a large sample of $\sim$300 DSFGs (J. McKinney et al. 2024; see also J. A. Hodge et al. 2024) show that the populations are large >1 kpc systems with extended disks and/or disturbed morphologies; all are detected in [F444W] brighter

than 26.5 AB magnitudes and have extended morphologies distinct from LRDs.

As an independent test of our derivation of dust masses using A_V and size, we apply the above method with the population of DSFGs from J. McKinney et al. (2024) that have dust detections, comparing dust masses derived from the submillimeter with those derived from NIRCam. We found consistent results within ± 0.6 dex, even though the dynamic range of dust masses of DSFGs is quite different than our estimates for LRDs.

Figure 1 shows the derived dust masses of the LRD sample, with mean dust mass $\langle M_{\rm dust}\rangle = (1.6^{+4.8}_{-0.9}) \times 10^4\,M_\odot$.

3.2. Dust Luminosities

Next we infer the bulk dust luminosities of the sample. This corresponds to the light that has been attenuated in the rest-frame UV/optical and reradiated at long wavelengths, commonly measured between rest-frame 8–1000 μm as $L_{\rm IR}$. In the absence of direct long wavelength constraints, energy balance implies that the difference between the observed and intrinsic UV luminosity is what should be absorbed by dust and reradiated at long wavelengths as $L_{\rm IR}$. How much light is absorbed relates to A_V.

In practice, $L_{\rm IR}$ may be found using the source's observed absolute UV magnitude $M_{\rm UV}$:

$$L_{\rm IR}(L_\odot) = (10^{0.4(4.83-M_{\rm UV})})(10^{0.4A_{\rm UV}} - 1), \quad (3)$$

where $A_{\rm UV}$ is the absolute magnitudes of attenuation at rest-frame UV magnitudes and $L_{\rm IR}$ given in $L_\odot$, and $M_{\rm UV}$ is the intrinsic emission expected in the UV from the *reddened* component of the SED. This differs from the faint blue emission that may be present in the rest-frame UV at much lower observed luminosities. The relationship between $A_{\rm UV}$ and A_V is a function of the attenuation curve; for Milky Way, LMC, and Calzetti dust attenuation curves, $A_{\rm UV}/A_V \approx 2.5$ (S. Salim & D. Narayanan 2020).

Note that we have made some simplified assumptions to get order-of-magnitude luminosities. First, we assume that the bolometric luminosity, in the absence of dust, is well approximated by the systems' UV luminosities. Also, as written, $L_{\rm IR}$ above corresponds to *all* reradiated dust emission, not just emission from 8 to 1000 μm, so a bolometric correction is needed. However, this correction factor is $\leqslant 1.2$ for all dust temperatures <200 K and $\leqslant 2$ at <300 K; this temperature range is appropriate for LRDs, as we will soon find.

Another way of estimating $L_{\rm IR}$ comes from SED measurements of SFRs and how much of that SFR is obscured by dust. Note that this is not entirely independent of other SED-derived characteristics like $M_{\rm UV}$ and A_V, but a slightly different set of assumptions serves as a worthwhile order-of-magnitude check. K. E. Whitaker et al. (2017) presents measurements of the obscured fraction of star formation, $f_{\rm obscured} \equiv {\rm SFR_{IR}}/({\rm SFR_{UV}} + {\rm SFR_{IR}})$ as a function of stellar mass, $M_\star$ for galaxies from $0 < z < 2.5$. They find no redshift evolution in $f_{\rm obs}(M_\star)$. Specifically, K. E. Whitaker et al. (2017) find

$$f_{\rm obscured} = (1 + a\exp(b\log_{10}(M_\star/M_\odot)))^{-1}, \quad (4)$$

where $a = (1.96 \pm 0.14) \times 10^9$ and $b = -2.277 \pm 0.007$. An SED-derived SFR can then be multiplied by $f_{\rm obscured}$ to obtain ${\rm SFR_{IR}}$; then using $\log(L_{\rm IR}/[L_\odot]) = \log({\rm SFR}/[M_\odot\ {\rm yr}^{-1}]) - 9.83$ (R. Kennicutt & N. Evans 2012) we get $L_{\rm IR}$. We note that the discrepancy between $L_{\rm IR}$ estimated via $M_{\rm UV}$ and A_V and that estimated via SFR and $M_\star$ has a scatter of $\sim$1 dex and systematic offset of $\sim$0.4 dex (such that the latter method estimates higher $L_{\rm IR}$ than the former). This is not entirely surprising given the known scatter about the K.E. Whitaker et al. (2017) relation and its possible evolution toward higher redshift (e.g., see D. T. Zimmerman et al. 2024). We estimate a mean IR luminosity for the LRD sample of $\langle L_{\rm IR}\rangle = (7.9^{+2.9}_{-4.7}) \times 10^{10}\,L_\odot$.

We emphasize that our ballpark estimates could be wildly incorrect for individual sources, but it should capture the bulk order-of-magnitude dust characteristics of the population as a whole. An extra note of caution comes, again, from highly obscured star-forming galaxies like DSFGs; it is not uncommon that energy balance can underestimate $L_{\rm IR}$, sometimes by up to 1 order of magnitude (A. Swinbank et al. 2004; E. da Cunha et al. 2015; C. Casey et al. 2017) when a clumpy ISM and high column densities lead to a "decoupling" of the optical-IR (OIR)/near-IR and dust SEDs. However, if such an underestimation were to apply for LRDs, it would be challenging to hide the additional luminosity; it would emerge either in the mid-IR (e.g., MIRI) if contained in a compact volume or in the submillimeter (e.g., Atacama Large Millimeter/submillimeter Array, ALMA) if spatially extended. Existing upper limits in both regimes suggest such an underestimate does not apply to LRDs.

3.3. Dust Temperatures

We derive IR SEDs (thus luminosity-weighted dust temperatures) by combining our newly derived constraints on $M_{\rm dust}$ and $L_{\rm IR}$. These SEDs are also neutral to interpretation as AGN or star formation as they are simple modified blackbodies. Specifically, we use a simple optically thin modified blackbody with a modest mid-IR power-law component ($\alpha_{\rm IR} = 4$) and emissivity spectral index $\beta = 2$ following the methodology described in C. M. Casey (2012) and subsequently P. M. Drew & C. M. Casey (2022). The dust mass is proportional to the flux density on the Rayleigh–Jeans side of the blackbody as well as the dust temperature, while the IR luminosity is proportional to the integral of the SED. These specific SED assumptions lead to a relation between dust temperature, IR luminosity, and dust mass of

$$T_{\rm dust}(K) = c\left(\frac{L_{\rm IR}}{L_\odot} \times \frac{M_\odot}{M_{\rm dust}}\right)^d, \quad (5)$$

where $c = 8.1 \pm 0.5$ and $d = 0.169 \pm 0.004$. The average luminosity-weighted dust temperature for the full sample is $\langle T_{\rm dust}\rangle = 110^{+21}_{-36}$ K.

There are many caveats regarding the relationship of dust temperature to peak wavelength, whether it is mass-weighted or luminosity-weighted or an optically thin or thick dust medium (C. Casey et al. 2014a; N. Scoville et al. 2016); however, the dust mass column densities we estimate here are only moderate, which allows for such simplified assumptions. By altering our set of assumptions on $\alpha_{\rm IR}$, β, and by propagating uncertainties from $M_{\rm dust}$ and $L_{\rm IR}$, the characteristic uncertainty on $T_{\rm dust}$ is $\sim$12 K.

One could, in principle, infer a dust temperature using the Stefan–Boltzmann Law; it is a factor of $\sim 2\times$ discrepant from

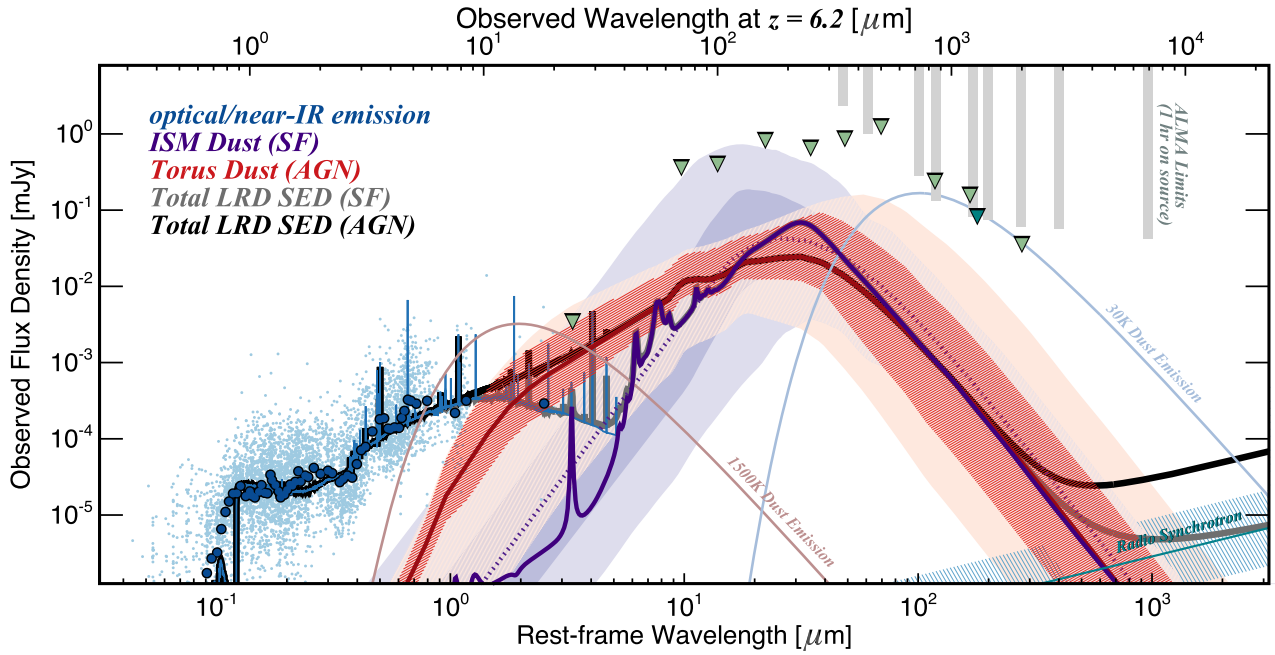

Figure 2. The average rest-frame UV through radio SED of the 675 LRDs in this work. The raw OIR/near-IR photometry of all LRDs is shown in light-blue points, the median stack in dark-blue points, and best-fit BAGPIPES model to the median stack by the thin blue line. The purple shaded region denotes the 68th and 95th percentile confidence regions on the derived dust SED discussed in Section 3, and the best-matched ∼100 K (B. Draine & A. Li 2007) model is shown in dark purple. The matching radio synchrotron component, assuming the FIR/radio correlation holds to high-z (V. Smolčić et al. 2017), is shown in teal with ±0.5 dex. The expectation for AGN torus emission is shown in orange, matched to the same predicted $L_{\rm IR}$ as the SED in Section 3. The total SED, summing optical/near-IR, dust, and synchrotron components, is shown in gray (using the Draine & Li star formation template) and black (using the Nenkova et al. torus template); both are made available. Measured 5σ limits in the mid/far-IR are shown in light-green triangles from A24 and from I. Labbe et al. (2023) in dark green. Vertical gray bars show the 5σ continuum depth achievable by ALMA in each of its observing bands with a 1 hr on-source integration time (as of ALMA Cycle 11 in 2024).

those we find in this work. An assumed condition of Stefan–Boltzmann is that the emergent luminosity has passed through an optically thick medium, which is likely not a valid presumption in the case of these systems; A. D. Burnham et al. (2021) present a detailed discussion of applying Stefan–Boltzmann to dust emission in galaxies (see their Sections 5.1 and 5.2.1).

4. The Dust SED of LRDs

4.1. SED Construction

We construct an average SED for LRDs from the rest-frame UV through the radio[8] using the combined aggregate LRD OIR photometry from HST/JWST provided in K24 and A24 and combine this with the dust SEDs derived in Section 3. The OIR SED is constructed by converting photometry to the rest frame using the best-fit photometric redshift for each LRD and using the isophotal wavelength of each filter to convert to effective wavelength of the photometric measurement; nondetections are included. Median stacks are calculated in bins with 100 photometric constraints below $\lambda_{\rm rest} < 8000$ Å and in two additional bins (with ∼20 measurements each) at longer wavelengths. The median OIR stack, converted back to observed flux density at the median sample redshift of $\langle z \rangle = 6.2$, is shown in dark-blue points on Figure 2.[9] We fit the stacked photometry using BAGPIPES (A. C. Carnall et al. 2018) with the same methodology as A24. Assuming no AGN contribution toward the rest-UV/optical SED, we infer an average stellar mass of $\langle M_\star \rangle = (8.1^{+3.1}_{-2.7}) \times 10^9\,M_\odot$ and attenuation $\langle A_V \rangle = 1.84 \pm 0.15$. We return to the issue of stellar mass in Section 4.3.

After generating individual, simple IR SEDs for all LRDs based on their inferred $M_{\rm dust}$ and $L_{\rm IR}$ in Section 3.3, we compute the median, 68th, and 95th inner confidence intervals, shown in purple on Figure 2. Our IR SED modeling is agnostic to heating mechanism—star formation or AGN—and thus does not include complex features from polycyclic aromatic hydrocarbon (PAH) and silicates.

In the case of a star-forming origin, we also overplot the best-matched realistic dust template to our median SED from B. Draine & A. Li (2007), which has a Milky Way extinction curve with 0.5% of dust from PAH molecules and a uniform incident radiation field with $U = 10^5$, i.e., 10^5 more intense than in the solar neighborhood's surrounding ISM. Based on the far-IR (FIR)/radio correlation, we also show the expected contribution of synchrotron emission from star formation following extrapolation from J. Delhaize et al. (2017).

Figure 2 shows the stark contrast of this average warm SED to a simpler, cold (∼30 K) modified blackbody oft used to model the dust component of star formation in the absence of direct FIR constraints (A. Pope et al. 2008; A. Swinbank et al. 2010; A. M. Swinbank et al. 2014; C. M. Casey 2020). Note that LRDs' SEDs are substantially warmer thanks to their compact sizes. Such low dust temperatures would only be feasible at lower dust surface densities (lower A_V) or more spatially extended emission. While the latter remains a possibility—implying that the OIR emission would be dwarfed

[8] Both average SEDs are made available on Github: https://github.com/caitlinmcasey/dust_in_lrds; a copy has been deposited to Zenodo: doi:10.5281/zenodo.13770534.

[9] Note this stack is very similar to the image-plane stack derived in A24 for LRDs, which is reassuring.

by a huge dust reservoir—such a system would be consistent with ∼kpc-scale DSFGs. As discussed in Section 3.1, all such DSFGs are spatially resolved at high SNR in F444W. Put another way, it should be quite surprising that *none* of these 600+ LRDs are detected as submillimeter galaxies (e.g., J. Simpson et al. 2019).

We also explore the relative expected emission from AGN tori independent of our simple derived SEDs from Section 3.3; the expected sublimation temperature of dust with mixed carbonaceous and silicate composition is ∼1500 K. A 1500 K modified blackbody with luminosity scaled from $L_{\rm bol}$ and A_V, assuming the OIR continuum is dominated by an AGN, is inconsistent with existing constraints on mid-IR emission from MIRI; most LRDs show a flat SED in F_ν extending to rest frame ∼2–3 μm. However, adopting a more complex emission model for a dusty torus from M. Nenkova et al. (2008) dramatically shifts the peak of the rest-frame SED to long wavelengths and relieves this tension with data. The M. Nenkova et al. (2008) SED shown in Figure 2 in red is the median of all $>10^6$ models in that work based on clumpy dust distributions around an AGN accretion disk. Its luminosity is normalized to the same luminosity expected ($L_{\rm IR}$), just now attributing its heating to AGN instead of star formation. The M. Nenkova et al. (2008) models are consistent with the AGN torus emission model developed by Z. Li et al. (2024) for LRDs, who presume a gray attenuation law (due to the destruction of small grains around AGN; see C. M. Gaskell et al. 2004) with an extended torus, which has the same effect as assuming a clumpy medium. In both cases, the SEDs peak at intrinsically longer wavelengths and relieve tension with the flat LRD SEDs measured with MIRI.

The relative consistency of the star-forming dust SED and the AGN torus dust SED is striking, especially because only the star-forming dust SED was derived using our energy balance and size measurement presented in Section 3. The M. Nenkova et al. (2008) models are built to accommodate a complex spatial distribution of dust clouds distributed in clumps, rather than a uniformly smooth and dense torus structure on $\lesssim$5 pc scales (see also discussion of obscuration of AGN from R. Maiolino et al. 2024). As a result, the mean luminosity-weighted temperature of the aggregate SED is ∼100 K, which is broadly consistent with what is expected from compact star formation on ∼50–100 pc scales. The only significance deviation between the two SEDs occurs at rest-frame ∼2–10 μm where the relative luminosity of hot dust is higher for tori. However, it is clear from Figure 2 that existing constraints in this regime are too few to discriminate between models when accounting for relevant uncertainties. Deep MIRI observations of LRDs will prove crucial to potentially detect torus emission, if present.

Note that assuming *smaller* sizes for LRDs $\ll$ 90 pc would drive the estimated dust masses down ($M_{\rm dust} \propto R_{\rm eff}^2$) and dust temperatures up ($T_{\rm dust} \propto R_{\rm eff}^{-2.169}$) such that sizes $\lesssim$25 pc predict peak dust temperatures that exceed the sublimation temperature and are in disagreement with current MIRI constraints.

4.2. Is the Dust Detectable with ALMA?

Figure 2 shows depths that can be reached at 5σ in each of the ALMA bands (1, 3, 4, 5, 6, 7, 8, 9, and 10) in an effective 8 GHz bandwidth with 1 hr of on-source integration time.[10] Unfortunately these limits (per source) reach sensitivities 2 orders of magnitude too shallow to detect direct dust emission from our predicted models. This unfortunately leaves direct dust detection via ALMA continuum observations unlikely for LRDs prior to ALMA's wideband receiver upgrade (to be completed ∼2030), as it would require either a factor of >20 increase in the sample size of LRDs to enable a stacking experiment on $>10^4$ sources or, alternatively, large investments in time (≫days) for very few sources.

4.3. Reconciling Stellar Mass with Dust Mass

The stellar mass we derive for the median OIR photometric stack is *high*, nearly $10^{10}\,M_\odot$: a factor of $\sim10^{5-6}$ larger than our estimated dust masses of LRDs. Note, of course, that this presumes all continuum light is stellar in nature, which may not be true. The expected maximum star-to-dust ratio one expects from supernovae and asymptotic giant branch star dust enrichment models is $\log(M_\star/M_{\rm dust}) \approx$ 3–4 (R. Schneider & R. Maiolino 2024). ISM grain growth would potentially lead to even lower star-to-dust ratios. If both mass estimates are accurate, then it may be likely that optically thick dust (and a patchy ISM geometry) could lead to the underestimation of the total dust mass. However, dust masses that are a factor of ∼100× larger would likely lead to *some* submillimeter detections among the sample, for which there are none (A24). The other (more likely) possibility is that stars do not dominate the continuum of LRDs. Put another way, we would expect stellar masses closer to $\sim10^{7-8}\,M_\odot$ by using our dust mass estimates and a $\log(M_\star/M_{\rm dust}) \approx$ 3–4; indeed, AGN light may dominate the rest-optical portion of the SED leading to systematic overestimation of the stellar mass (see the spectroscopic analysis from B. Wang et al. 2024b).

5. Volume Constraints

While the dust reservoirs in LRDs by our estimation are expected to be rather modest in mass ($\sim10^{4-5}\,M_\odot$), the relative volume density of LRDs means that they could plausibly represent the lion's share of dust to have formed at early times, within the Universe's first ∼2 Gyr. Do they? To test this hypothesis, we calculate the dust mass volume density with redshift estimated for the LRDs in this work and compare against estimates for DSFGs (A. Blain et al. 2002; C. Casey et al. 2014a). To infer the latter, we use the C. Casey et al. (2018) model framework for building realizations of the IR luminosity function and their associated (sub)millimeter emission. Specifically, we adopt the measured luminosity function parameters from J. A. Zavala et al. (2021) relevant for the $z > 2$ Universe, simulate a 100 deg^2 light cone, then model the dust mass of each contributor to the IRLF to directly calculate the implied dust mass volume density. The associated total dust mass density curves are shown for all $>10^9\,L_\odot$ galaxies, all LIRGs, and all ULIRGs in Figure 3. Other measurements of the dust mass volume density are shown for context, extending out to $z \sim 5$ from C. Péroux & J. C. Howk (2020).

Using a total survey area of 0.5 deg^2 for the A24 LRD sample and 640 arcmin^2 for that of K24, we compute the direct contribution of these 675 LRDs to the dust mass volume

[10] Calculated using the Cycle 11 version of the ALMA Observing Tool, Doc. 11.5, version 1.0.

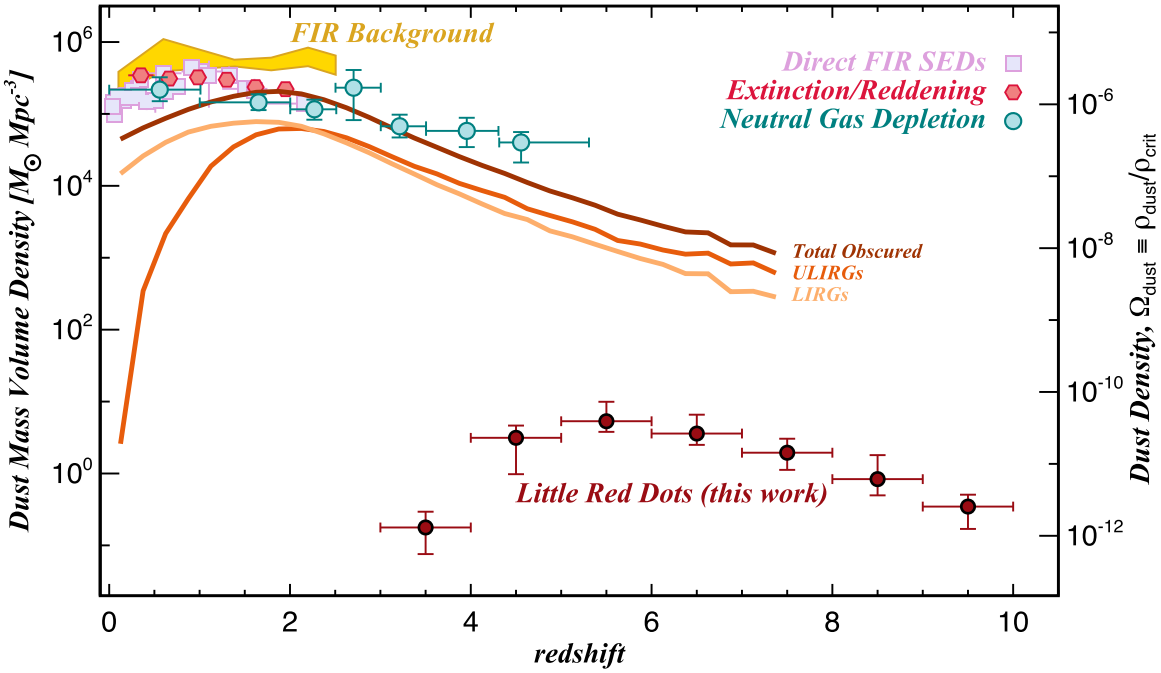

Figure 3. The dust mass volume density of the Universe placing LRDs (dark red) in context. Measurements presented in the literature are made from the FIR background directly (yellow; C. Thacker et al. 2013), galaxies with directly observable FIR SEDs (lavender; L. Dunne et al. 2011; R. A. Beeston et al. 2018; S. P. Driver et al. 2018; F. Pozzi et al. 2020), extrapolation from extinction/reddening of OIR SEDs (light red; B. Ménard et al. 2010; B. Ménard & M. Fukugita 2012), and neutral gas depletion (teal; C. Péroux & J. C. Howk 2020). We overplot the integrated contribution from IR luminous galaxies with $L_{IR} > 10^9\,L_\odot$ in brown, and specifically from ULIRGs (orange; $L_{IR} > 10^{12}\,L_\odot$) and LIRGs (tan; $10^{11} < L_{IR} < 10^{12}\,L_\odot$) from the C. Casey et al. (2018) model, using the measured luminosity function parameters from J. A. Zavala et al. (2021). Despite their relatively high number density, LRDs are thought to only contribute ∼0.1% to the cosmic dust budget relative to the total, which is dominated by IR luminous galaxies.

density to be on the order of 1–10 $M_\odot$ Mpc^{-3} (see Figure 3). This is 2–3 orders of magnitude lower than the expected contributions from the more spatially rare DSFG population at similar epochs. This indicates that the LRD population, despite being a relatively common phenomenon, does not contribute significantly to the cosmic dust budget given that individually their masses are quite low, $\sim 10^{4-5}\,M_\odot$. While DSFGs are a much more dominant contributor at $z \sim 5$–7, it is important to remember that DSFGs themselves are more rare but have dust reservoirs that are individually 100–1000× more massive than estimated for LRDs.

6. Summary

We have used two large literature samples of LRDs to put basic constraints on their dust characteristics. We use measured A_V, M_{UV}, and R_{eff} to derive dust masses, luminosities, and temperatures. Given their compact morphologies, their dust masses are estimated to be relatively small, averaging $\langle M_{dust}\rangle = (1.6^{+4.8}_{-0.9}) \times 10^4\,M_\odot$, with luminosities $\langle L_{IR}\rangle = (8^{+3}_{-5}) \times 10^{10}\,L_\odot$ and dust temperatures $\langle T_{dust}\rangle = 110^{+21}_{-36}$ K. Such dust properties would imply that current ALMA observational limits on LRDs are 2 orders of magnitude too shallow to render a detection.

While the nature of dust in LRDs is often thought of as a dichotomy—either embedded in a nuclear torus on ∼pc scales and temperatures ∼1500 K or diffuse on ∼100 pc scales in the ISM with temperature ∼30 K—we find that expectation for dust emission from clumpy torus models (M. Nenkova et al. 2008) is fully consistent with the predicted dust heated via star formation in the ISM, both peaking at rest frame ∼20–40 μm. This convergence of AGN and ISM dust models is due to LRDs' compact size (driving the ISM dust to be hotter than "normal" ISM dust) and that complex clumpy torus dust models lead to cooler dust emission (when weighted by luminosity) than might nominally be expected.

The star-to-dust mass ratios inferred for LRDs ($\sim 10^{5-6}$) are much higher than expected for typical dust formation scenarios ($\sim 10^{3-4}$). Either AGNs contribute significantly to the rest-optical emission of LRDs (J. E. Greene et al. 2024; B. Wang et al. 2024a), resulting in an overestimation of the stellar mass if fit directly to the continuum, or dust masses are significantly higher than predicted here, leaving the possibility that *some* may be detectable via dust continuum with ALMA.

Given the modest predicted dust masses in LRDs, we find they contribute only negligibly (∼0.1%) to the cosmic dust budget, dwarfed by the contribution from DSFGs that is a factor of $\gtrsim$10× more rare but with $\gtrsim$100–1000× higher dust mass.

Acknowledgments

We are grateful to the anonymous referee and to Justin Spilker, Jorge Zavala, and Seiji Fujimoto for the helpful discussions that improved the manuscript. C.M.C. thanks the National Science Foundation for support through grants AST-2009577 and AST-2307006 and to NASA through grant JWST-GO-01727 awarded by the Space Telescope Science Institute, which is operated by the Association of Universities for Research in Astronomy, Inc., under NASA contract NAS 5-26555. H.B.A. acknowledges support from the Harrington Graduate Fellowship at UT Austin, and H.B.A. and O.R.C. thank the National Science Foundation for support from Graduate Research Fellowship Program awards. V.K. acknowledges support through UT's Cosmic Frontier Center as an

inaugural CFC Postdoctoral Fellow, and J.M., A.S.L., and S.M. M. thank NASA for their support through the Hubble Fellowship Program.

Authors from UT Austin acknowledge that they work at an institution that sits on indigenous land. The Tonkawa lived in central Texas, and the Comanche and Apache moved through this area. We pay our respects to all the American Indian and Indigenous Peoples and communities who have been or have become a part of these lands and territories in Texas.

ORCID iDs

Caitlin M. Casey https://orcid.org/0000-0002-0930-6466
Hollis B. Akins https://orcid.org/0000-0003-3596-8794
Vasily Kokorev https://orcid.org/0000-0002-5588-9156
Jed McKinney https://orcid.org/0000-0002-6149-8178
Olivia R. Cooper https://orcid.org/0000-0003-3881-1397
Arianna S. Long https://orcid.org/0000-0002-7530-8857
Maximilien Franco https://orcid.org/0000-0002-3560-8599
Sinclaire M. Manning https://orcid.org/0000-0003-0415-0121

References

Akins, H. B., Casey, C. M., Lambrides, E., et al. 2024, arXiv:2406.10341
Aniano, G., Draine, B. T., Calzetti, D., et al. 2012, ApJ, 756, 138
Antonucci, R. 1993, ARA&A, 31, 473
Baggen, J. F. W., van Dokkum, P., Brammer, G., et al. 2024, arXiv:2408.07745
Bagley, M. B., Finkelstein, S. L., Koekemoer, A. M., et al. 2023, ApJL, 946, L12
Beeston, R. A., Wright, A. H., Maddox, S., et al. 2018, MNRAS, 479, 1077
Blain, A., Smail, I., Ivison, R., Kneib, J., & Frayer, D. 2002, PhR, 369, 111
Bohlin, R., Savage, B., & Drake, J. 1978, ApJ, 224, 132
Burnham, A. D., Casey, C. M., Zavala, J. A., et al. 2021, ApJ, 910, 89
Carnall, A. C., McLure, R. J., Dunlop, J. S., & Davé, R. 2018, MNRAS, 480, 4379
Casey, C., Cooray, A., Killi, M., et al. 2017, ApJ, 840, 101
Casey, C., Narayanan, D., & Cooray, A. 2014a, PhR, 541, 45
Casey, C., Zavala, J., Spilker, J., et al. 2018, ApJ, 862, 77
Casey, C., Scoville, N. Z., Sanders, D. B., et al. 2014b, ApJ, 796, 95
Casey, C. M. 2012, MNRAS, 425, 3094
Casey, C. M. 2020, ApJ, 900, 68
Casey, C. M., Kartaltepe, J. S., Drakos, N. E., et al. 2023, ApJ, 954, 31
da Cunha, E., Walter, F., Smail, I., et al. 2015, ApJ, 806, 110
Delhaize, J., Smolčić, V., Delvecchio, I., et al. 2017, A&A, 602, A4
Diplas, A., & Savage, B. D. 1994, ApJS, 93, 211
Draine, B., Dale, D., Bendo, G., et al. 2007, ApJ, 663, 866
Draine, B., & Li, A. 2007, ApJ, 657, 810
Draine, B. T., Aniano, G., Krause, O., et al. 2014, ApJ, 780, 172
Drew, P. M., & Casey, C. M. 2022, ApJ, 930, 142
Driver, S. P., Andrews, S. K., da Cunha, E., et al. 2018, MNRAS, 475, 2891
Dunne, L., Gomez, H. L., da Cunha, E., et al. 2011, MNRAS, 417, 1510
Eisenstein, D. J., Johnson, B. D., Robertson, B., et al. 2023a, arXiv:2310.12340
Eisenstein, D. J., Willott, C., Alberts, S., et al. 2023b, arXiv:2306.02465
Gaskell, C. M., Goosmann, R. W., Antonucci, R. R. J., & Whysong, D. H. 2004, ApJ, 616, 147
Greene, J. E., Labbe, I., Goulding, A. D., et al. 2024, ApJ, 964, 39
Güver, T., & Özel, F. 2009, MNRAS, 400, 2050
Hickox, R. C., & Alexander, D. M. 2018, ARA&A, 56, 625
Hodge, J. A., da Cunha, E., Kendrew, S., et al. 2024, arXiv:2407.15846
Hopkins, P. F., Murray, N., Quataert, E., & Thompson, T. A. 2010, MNRAS, 401, L19
Howell, J., Armus, L., Mazzarella, J., et al. 2010, ApJ, 715, 572
Kennicutt, R., & Evans, N. 2012, ARA&A, 50, 531
Kocevski, D. D., Finkelstein, S. L., Barro, G., et al. 2024, arXiv:2404.03576
Kocevski, D. D., Onoue, M., Inayoshi, K., et al. 2023, ApJL, 954, L4
Kokorev, V., Caputi, K. I., Greene, J. E., et al. 2024, ApJ, 968, 38
Kreckel, K., Groves, B., Schinnerer, E., et al. 2013, ApJ, 771, 62
Labbe, I., Greene, J. E., Bezanson, R., et al. 2023, arXiv:2306.07320
Labbe, I., van Dokkum, P., Nelson, E., et al. 2023, Natur, 616, 266
Li, Z., Inayoshi, K., Chen, K., Ichikawa, K., & Ho, L. C. 2024, arXiv:2407.10760
Maiolino, R., Risaliti, G., Signorini, M., et al. 2024, arXiv:2405.00504
Matthee, J., Naidu, R. P., Brammer, G., et al. 2024, ApJ, 963, 129
McKinney, J., Casey, C. M., Long, A. S., et al. 2024, arXiv:2408.08346
Ménard, B., & Fukugita, M. 2012, ApJ, 754, 116
Ménard, B., Scranton, R., Fukugita, M., & Richards, G. 2010, MNRAS, 405, 1025
Misgeld, I., & Hilker, M. 2011, MNRAS, 414, 3699
Nenkova, M., Sirocky, M., Ivezić, Ž., & Elitzur, M. 2008, ApJ, 685, 147
Oesch, P. A., Brammer, G., Naidu, R. P., et al. 2023, MNRAS, 525, 2864
Péroux, C., & Howk, J. C. 2020, ARA&A, 58, 363
Peterson, B. M. 2006, in Physics of Active Galactic Nuclei at all Scales, ed. D. Alloin, Vol. 693 (Berlin: Springer), 77
Pope, A., Chary, R., Alexander, D., et al. 2008, ApJ, 675, 1171
Pozzi, F., Calura, F., Zamorani, G., et al. 2020, MNRAS, 491, 5073
Rémy-Ruyer, A., Madden, S., Galliano, F., et al. 2014, A&A, 563, A31
Salim, S., & Narayanan, D. 2020, ARA&A, 58, 529
Schneider, R., & Maiolino, R. 2024, A&ARv, 32, 2
Scoville, N., Sheth, K., Aussel, H., et al. 2016, ApJ, 820, 83
Shen, X., Hopkins, P. F., Faucher-Giguère, C.-A., et al. 2020, MNRAS, 495, 3252
Simpson, J., Smail, I., Swinbank, A., et al. 2019, ApJ, 880, 43
Smolčić, V., Novak, M., Bondi, M., et al. 2017, A&A, 602, A1
Swinbank, A., Smail, I., Chapman, S., et al. 2004, ApJ, 617, 64
Swinbank, A., Smail, I., Longmore, S., et al. 2010, Natur, 464, 733
Swinbank, A. M., Simpson, J. M., Smail, I., et al. 2014, MNRAS, 438, 1267
Thacker, C., Cooray, A., Smidt, J., et al. 2013, ApJ, 768, 58
Wang, B., de Graaff, A., Davies, R. L., et al. 2024a, arXiv:2403.02304
Wang, B., Leja, J., de Graaff, A., et al. 2024b, ApJL, 969, L13
Whitaker, K. E., Pope, A., Cybulski, R., et al. 2017, ApJ, 850, 208
Williams, C. C., Alberts, S., Ji, Z., et al. 2024, ApJ, 968, 34
Williams, C. C., Tacchella, S., Maseda, M. V., et al. 2023, ApJS, 268, 64
Zavala, J. A., Casey, C. M., Manning, S. M., et al. 2021, ApJ, 909, 165
Zimmerman, D. T., Narayanan, D., Whitaker, K. E., & Davè, R. 2024, ApJ, 973, 146